Research Article | Vol. 29, No. 26 / 20 Dec 2021 / Optics Express 42900
Optics EXPRESS

Information advantage from polarization-multiplexed readout of nanophotonic scattering overlay sensors

ROBIN D. BUIJS,[1] TOM A. W. WOLTERINK,[1] GIAMPIERO GERINI,[2,3] A. FEMIUS KOENDERINK,[1] AND EWOLD VERHAGEN[1,*]

[1] Center for Nanophotonics, AMOLF, Science Park 104, 1098 XG Amsterdam, The Netherlands
[2] Optics Department, Netherlands Organization for Applied Scientific Research (TNO), Stieltjesweg 1, 2628 CK Delft, The Netherlands
[3] Department of Electrical Engineering, Technische Universiteit Eindhoven (TU/e), 5600 MB Eindhoven, The Netherlands
[*] e.verhagen@amolf.nl

Abstract: Nanophotonic structures are powerful tools for sensing, with the goal of retrieving parameters accurately at maximum speed and minimum photon budget. As information on those parameters can be distributed over multiple output scattering channels that propagate to the far field, considering well-chosen combinations of far-field optical degrees of freedom could benefit measurement precision. We explore how multiplexing readout across different polarization channels enhances parameter retrieval in nanophotonic overlay sensors. We measure the relative position between layers with nanoscale scattering structures, known as overlay in semiconductor metrology, and show that multiplexing either incident or analyzed polarization leads to improved parameter retrieval in the systems studied. At fixed photon budget, we extract additional information equivalent to more than 7 dB in signal level. These results demonstrate that significant advantages in measurement performance of nano-optical sensors can be gained by exploiting the vectorial nature of optical fields.

1. Introduction

Nanophotonic devices are known as excellent sensors in (bio)molecular detection and spectroscopy [1–4], thanks to nanoscale field confinement and the availability of high-quality quantum-limited light sources and detectors. The complexity of optical far-fields also makes nanophotonic sensors exquisitely suited for multi-parameter retrieval problems. Examples of multi-parameter retrieval problems range from few-parameter problems like overlay measurement, which measures in-plane positioning error between two fabricated layers in terms of two parameters (X and Y), to imaging, with parameters for each of possibly millions of pixels. Overlay measurement, a technique crucial to continued semiconductor device miniaturization [5–9], is commonly performed using sets of overlapping gratings, with nanophotonic models used to extract overlay and other process parameters from scatterometry data [10–15]. Likewise, computational imaging retrieves complex spatial optical information from non-imaging detection set-ups [16–22], with localized surface plasmon assisted structured illumination microscopy in particular exploiting nearby nanophotonic scattering structures in image reconstruction [23,24]. Multi-parameter retrieval problems are thus of widespread fundamental and practical interest.

The optical far field is a high-dimensional concept, with information contained in wavevector, frequency and polarization degrees of freedom. Information from different channels must be combined to resolve the parameters in complex parameter retrieval problems. Various strategies exist to solve the inverse problem of retrieving scattering parameters from the resulting light fields [25–28]. In order to retrieve information optimally efficiently, we need to understand how

#446346 https://doi.org/10.1364/OE.446346
Journal © 2021 Received 21 Oct 2021; revised 18 Nov 2021; accepted 25 Nov 2021; published 8 Dec 2021

Optics EXPRESS

precisely nanoscopic information on the scattering system is encoded in far-field channels. Of particular interest is polarization information, which is often disregarded through polarization-agnostic measurement schemes. Mueller polarimetry, which resolves the full 4×4 matrix that describes polarization transfer through a sample [29,30], provides a wealth of information about sample structure [9,31]. The power of polarimetry is further enhanced when combined with other information channels, for instance as in angle-resolved polarimetry [32]. However, full reconstruction of the polarization matrix may not be needed to combine polarization information with other degrees of freedom. The key question is how information from some particular degree of freedom can be exploited optimally to improve parameter estimates in any specific problem.

In this work, we show that for a given photon budget, more precise nanophotonic parameter retrieval can be performed through polarization multiplexing than from unpolarized measurements. We illustrate our approach by applying it to the task of pattern overlay measurement. We measure overlay error on few-nanoparticle scattering sensors and aim to optimize measurement precision, considering several strategies for multiplexing light polarization in input and output channels. Applying a calibration-based method to retrieve overlay from devices with a wide range of overlay errors, we compare the performance of the different strategies to quantify the information gained by combining polarization channels. We explore the dependence of measurement precision on photon budget through a discrete dipole model and analyze both theoretically and in experiment how overlay performance for different strategies relates to wavevector resolution. Finally, we discuss how combining information from different polarization channels may benefit nano-optical sensing more broadly.

2. Method

We study polarization multiplexing by applying it to the retrieval of the two-dimensional location of a single nanoparticle above a layer with fixed nanoscale structure. This task is a model example of overlay measurement, where we consider two layers of a sample that have a small but unknown in-plane displacement with respect to the design, as a result of fabrication tolerances. The challenge is to measure this displacement, known as the overlay error [5–9]. We use overlay targets with an exceptionally small footprint of only 400 nm to a side, consisting of four nominally identical gold discs of thickness 40 nm and diameter 110 nm. These structures have previously been shown to be suitable for overlay measurement, in spite of their small size and the fabrication imperfections arising from prototyping using electron-beam lithography [33]. Such particles have a plasmonic resonance at a wavelength around 700 nm, around which wavelength they strongly scatter incident light. We use a layout with three particles in the bottom layer, arranged in an L-shape, and a solitary particle in the top layer, all embedded in commercial spin-on glass (MicroResist Ormocomp) with the layers separated by approximately 89 nm. This system is studied optically from below, as sketched in Fig. 1(a). The overlay error in this target is the in-plane distance from the midpoint between opposite particles in the bottom layer, to the midpoint of the particle in the top layer. The relevant displacements and axes are indicated on a scanning electron image of one such structure in Fig. 1(b). This design breaks the symmetry between some of the axes, such as D and A, without breaking that between H and V unless the top-layer particle does so. This may lead to some polarizations, or combinations thereof, providing more sensitive overlay measurements than others. We fabricate such targets with a wide range of relative displacements. Devices lie on a grid where both X and Y overlay nominally range from -187.5 nm to 187.5 nm in 37.5 nm steps. Fabrication produced a constant offset of around 15 nm and nanometer-scale fabrication errors on top of that. We will refer to these engineered overlay errors as overlay values. The grid allows us to verify our overlay measurement performance over this entire parameter range and compare the different polarization readout strategies.

Optics EXPRESS

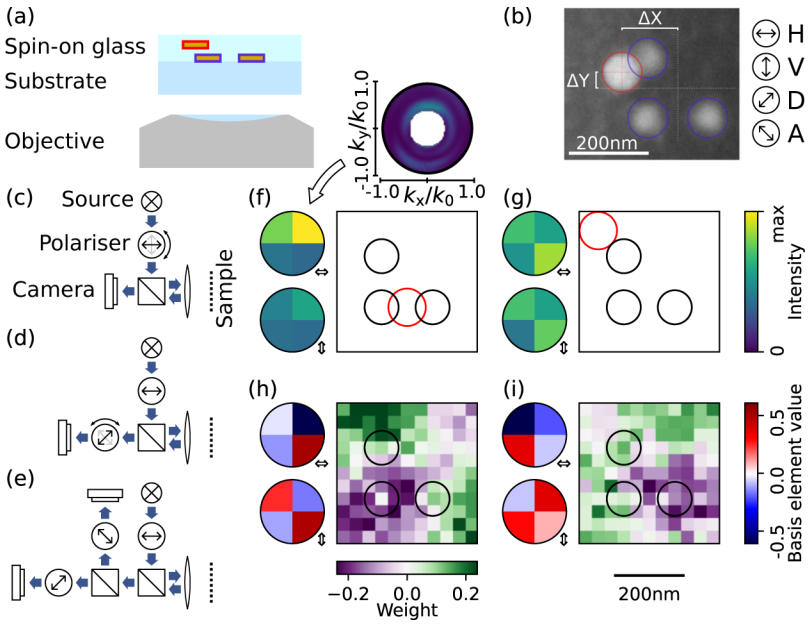

Fig. 1. (a) Schematic cross-section of device, showing arrangement of layers and objective. (b) Scanning electron image showing overlay error on an overlay target: zero overlay occurs when the red cross, centred on the red-circled particle, overlaps with the white cross, centred between the blue-circled particles. Circled arrows define the polarization axes in the same XY frame as the electron image. (c)-(e) Three strategies for polarization multiplexed measurement, either (c) changing an input polarizer between measurements, (d) changing an analysis polarizer between measurements or (e) reading out two polarization channels in parallel. (f)-(g) Example measurements using quadrant detectors in two input polarization channels. Circular panels show detector pixel intensities, square panels show the relative arrangement of particles that produced this reading. Inset: the full-resolution masked radiation pattern integrated to obtain one of the four-pixel datasets. (h)-(i) Two entries from the singular value decomposition of a full reference set for 11×11 overlay values. Circular panels show pixel intensity components corresponding to this basis element, square panels show the weight this basis element has for each position of the fourth particle.

There are several possible strategies for measuring complementary far-field polarization channels for a static sample structure. In the first we consider polarizing a beam of light before directing it to a sample. The reflected (or transmitted) light is captured on a detector. By rotating the input polarizer, the sample response to light of complementary polarizations may be measured separately, as sketched in Fig. 1(c). Both independent measurements can then be used together to address the overlay problem. We refer to this approach as input polarization multiplexing. Alternatively, the sample may be illuminated with light of a fixed polarization, or with unpolarized light, whereupon the reflected light is analyzed along different polarization axes. This analysis may be performed in series by rotating an analyzer, in analogy with the input polarization multiplexing scenario, as sketched in Fig. 1(d). Alternatively, both channels may be measured at once by employing a beam splitter and two analyzers (or a polarizing beam splitter), as sketched in Fig. 1(e). We refer to the latter two strategies as output polarization multiplexing. We wish to explore how input and output polarization multiplexing compare to standard approaches that use a single fixed polarization or unpolarized light, as well as to each other.

Optics EXPRESS

In our measurements, we collect radiation patterns with a detector in a Fourier plane, thus measuring radiant flux versus parallel wavevector (k_x, k_y). The sample is illuminated with supercontinuum laser light (NKT Whitelase Micro) filtered down to a 10 nm band around 620 nm. This light is used to illuminate the target with $NA_{in} = 0.37$ and the part of Fourier space corresponding to specular reflection of the illuminating light is blocked from detection. The detector is divided into a number of square pixels, capturing light up to the numerical aperture of our objective $NA_{out} = 0.95$. We will mostly consider measurements made with an effective quadrant (four-pixel) detector, with the radiation pattern centred on the detector, so that all pixels show equal intensity in the case of a symmetric radiation pattern. We implement such a detector experimentally by projecting Fourier images onto a camera (Basler ACA1920-40UM) and integrating the counts in each quadrant of the observed back focal plane image, as acquired over an integration time of 40 ms. This produces four pixel values per measurement in the case of traditional single-polarization measurements and eight in polarization-multiplexed cases. We collect far-field data for the full grid of overlay values available on the sample. Two example measurements for different overlay values are shown in Fig. 1(f) and 1(g). Circular panels show intensity on each segment of the quadrant detectors for horizontal (top) and vertical (bottom) polarization.

The measured intensities are the result of an interplay of scattering events within the device. We opt for a calibration-based method to retrieve overlay error from these intensity patterns. Unlike forward theoretical modelling, such calibration-based methods handle realistic fabrication artefacts and parasitic reflections without complication. The calibration-based method we use to extract overlay value from far-field data was previously used to localize point-like light sources [34] and scattering objects [35]. It requires one reference measurement per resolvable value in the calibrated domain. In this case, this means one measurement for each overlay value in the sample grid. Each such measurement is used as a row in a signals matrix A. Singular value decomposition (SVD) allows any such matrix A to be rewritten as $A = U\Sigma V^*$, where the asterisk represents conjugate transposition, with U and V unitary matrices and Σ diagonal [36]. Singular value decomposition finds the principal components of the data set, giving us basis vectors such that each next basis vector has maximum overlap with the part of the data not captured in previous basis vectors. Practically, this means that complex datasets can be captured in just a few basis elements [34].

Two elements of such an optimal basis, from the singular value decomposition of the data collected on the full grid before, are shown in Figs. 1(h) and 1(i). Circular panels show the value of the basis elements at each pixel for either polarization. Square panels show the weight these basis elements have at each position in the reference set. There are as many basis elements as pixels, but only a few have appreciable weight anywhere. The examples shown are interesting because they have large weight, but also a smooth dependence of weight on position, with broad, contiguous regions of positive or negative weight. Importantly, each of the basis elements has different pixel values for the two polarization channels. This means that being able to resolve the polarization channels may provide additional information: there is a difference that would have washed out in a single-polarization or unpolarized light measurement.

3. Results

We use this calibration-based method to reconstruct overlay from new data, i.e. independent measurements that may differ from the calibration data because of varying noise and/or instrumental deviations. In order to illustrate the qualitative behavior of the method, we first turn to a theoretical model. We use a discrete dipole approximation, where the overlay target is modelled as four point scatterers of polarizability $|\alpha| = 5.56 \times 10^{-33}$ C m^{2}V^{-1} and a quality factor $Q = 10$ in a homogeneous medium. Discrete dipole models let us quickly estimate the qualitative behavior of sets of interacting particles [37–40], taking into account multiple scattering, self-action and

Optics EXPRESS

retardation [41,42]. We can calculate far-field data on quadrant detectors and analyze them in much the same way as for the experimental data. We specifically include synthetic shot noise for the appropriate photon budget, around $N = 10^6$, which corresponds to the integrated intensity over all pixels in all measured polarization channels. We calculate far-field data for a large grid of overlay values, 2λ in 31 steps to a side, and take their singular value decomposition. This constitutes our reference library. Next, we calculate a new set of data, with independent noise, to mimic an independent measurement. We project these new data onto the optimal basis and compare the coefficients with those for the positions in our reference library through the least square of residuals. The reference position corresponding to the best match is taken as the overlay value estimate. In Fig. 2(a) we show the error in such estimates for one full set of newly generated test data using input polarization multiplexing, projected onto the optimal basis. Some patterns can be seen in these noisy data, with retrieval errors largest in the corners and along the symmetry axes of the quadrant diode. We can average many (n_i) instances to find an average error $\Delta\mathrm{OV}_\mathrm{a}$ at some overlay value (x, y):

$$\Delta\mathrm{OV}_{\mathrm{a},xy} = \frac{1}{n_i}\sum_i |v_i|, \tag{1}$$

where v_i are the individual error vectors between the estimated and correct overlay value, for each instance i. Averaging 300 instances of the error map from Fig. 2(a), with different noise realizations, produces the average error map in Fig. 2(b). We see some fine structure in average error versus overlay, but mainly observe that overlay performance is best for small overlay value. We can now rephrase our original challenge: we intend to find out if and how such average error maps improve with the introduction of polarization multiplexing at constant total photon budget.

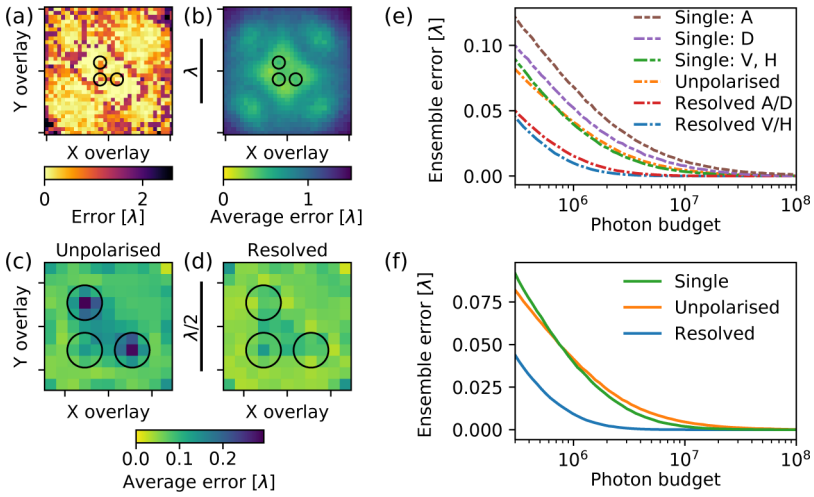

Fig. 2. Overlay retrieval in theoretical polarization multiplexing. (a) Overlay retrieval error versus overlay value for one set of noisy synthetic data. (b) Average error versus overlay value for the scenario used in (a). (c-d) Average error versus position for experimentally relevant library dimensions, for (c) unpolarized detection and (d) H-V input polarization resolved detection. (e) Ensemble error versus photon budget for a range of input polarization multiplexing strategies, with library dimensions as in (c). (f) Overlay retrieval in theoretical output polarization multiplexing. Ensemble error calculated as a function of photon budget for a range of polarization strategies, using a library of the same dimensions as in experiment.

We first test input polarization multiplexing in theory. We consider the same overlay values available in experiment and calculate average error for two polarization strategies: unpolarized light and input polarization multiplexing between H and V polarization (as defined in Fig. 1)

Optics EXPRESS

for the same total photon budget. The consideration of constant photon budget means that any advantage of multiplexing would imply that the incorporation of another polarization channel is more valuable to overlay retrieval than integrating twice as long. We calculate average error versus overlay and, as can be seen in Figs. 2(c) and 2(d), average error is appreciably lower with polarization resolution than without. In some cases, polarization resolution appears to allow distinguishing between some non-unique solutions, like directly below the outer particles in the bottom layer. Practically all positions show an improvement in average error. We can further analyze these data by averaging the error maps across all overlay values to produce an ensemble error $\Delta\mathrm{OV_e}$:

$$\Delta\mathrm{OV_e} = \frac{1}{n_x n_y} \sum_{(x,y)} \Delta\mathrm{OV_{a,}}_{xy}, \tag{2}$$

for all $n_x \times n_y$ pairs of overlay value (x, y) in the library. This ensemble error depends on the size and density of the library, but may be compared with ensemble errors for libraries with the same dimensions. The ensemble error for given library dimensions will be a function not only of the polarization multiplexing strategy used, but also of the available photon budget. We calculate this ensemble error over a range of photon budgets and for the polarizations used before, as well as multiplexing between D and A polarizations and all corresponding single polarizations. We compare three scenarios of unpolarized input, single-polarization input (A, D, V, H), and polarization-resolved input (A-D, V-H), all having polarization-insensitive detection. The results of these ensemble average calculations, plotted in Fig. 2(e), show the two multiplexed strategies drastically outperforming both unpolarized and single-polarization measurements. As a rule, the V-H polarization channels and their combinations perform a bit better than the A-D ones, but the difference is small compared to the large advantage from polarization multiplexing, which corresponds to an effective improvement in photon budget of around 7 dB for photon budgets around 3×10^5: the performance obtained with multiplexed data would otherwise require four times the acquisition time.

Due to the nature of the calibration-based method used, average and ensemble errors depend on the size and density of the library. The largest possible average error corresponds to $\sqrt{2}(N-1)$ steps for a square library of $N \times N$ positions. Moreover, even without any signal, we can achieve an ensemble error of only around half the library width by guessing all data were taken at the library center. This is likely to limit observed ensemble error at very small photon budgets. Our method thus is only valid in the regime of ensemble errors small compared to the width of the library. This is the case for the ensemble errors in Fig. 2(e), so we do not expect these to be affected by the finite size of the library. Instead, we observe clear differences between polarization strategies. This improved performance of the polarisation resolved data in the discrete dipole model predicts that polarisation multiplexed measurement will result in a significant improvement in overlay retrieval performance.

We test this hypothesis in experiment by measuring overlay value with different polarisation strategies. As a reference library we use the previously-acquired data set of Fig. 1, of which two elements of the singular value decomposition are shown in Figs. 1(h) and 1(i). Now, we collect a new set of measurements on the same structures and project these measurements onto the reference library. We estimate the overlay value using the library and calculate the overlay retrieval error. In Fig. 3(a) and 3(b), we show such error maps for unpolarized and V-H resolved measurements. Unlike in the theoretical case (Fig. 2(c)), we do not directly recognize the shape or orientation of the overlay target in the data. It is likely that fabrication errors or experimental details dominate the pattern of errors, as both are expected to be large with few-nanoparticle overlay targets. Nonetheless, we see a drastic improvement in overlay retrieval performance from including polarization information when comparing the unpolarized case to the polarization-resolved one. We repeat this experiment on different realizations of the same set of structures. When we calculate ensemble error for each set of such measurements, as well

Optics EXPRESS

as for single-polarization measurements (the same combinations of polarizations as in theory), we find the results shown in Fig. 3(c). These results confirm the improvement in performance: single-polarization and unpolarized measurements perform similarly, but polarization-resolved measurements perform much better, with average ensemble error across a series of measurements going from around 70 nm (two library steps) to around 10 nm (a fraction of one library step). This improvement is greater than the improvement found at similar ensemble error in the theoretical results (Fig. 2(e)). This may be because experimental performance is limited by other sources of error than shot noise, the only noise source included in the theory. The experimental data confirm that input polarization multiplexing can drastically improve the precision of measurement of a parameter of a scattering system, as applied to overlay retrieval here.

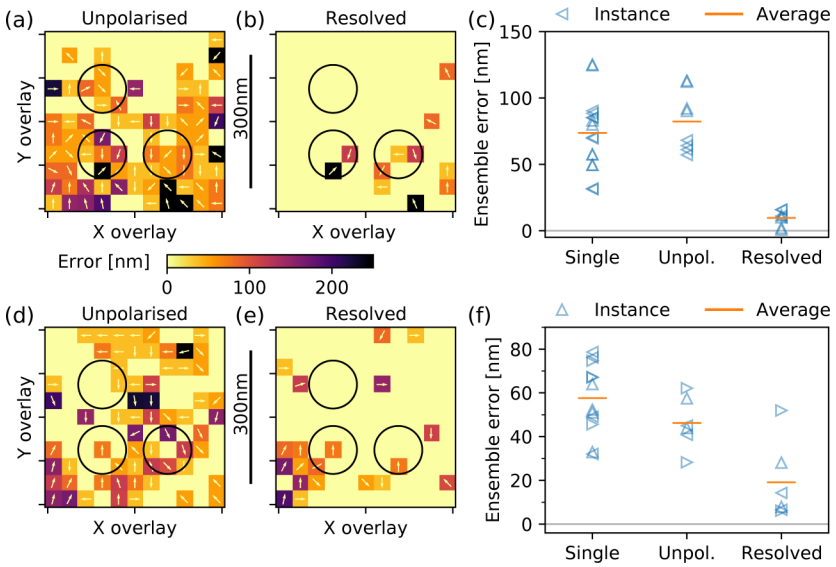

Fig. 3. Overlay retrieval in experimental input (a-c) and output (d-f) polarization multiplexing. (a-b) Overlay retrieval error for (a) unpolarized detection and (b) H-V polarization resolved detection. Dimensions are the same as in Fig. 2(c). (c) Ensemble error for experimental data versus polarization strategy: a single fixed polarization, unpolarized illumination and detection and resolved orthogonal polarization channels. Differently oriented triangles correspond to different devices under test, averages are calculated across all data for a given polarization strategy. (d-f) Like (a-c), but using output polarization multiplexing.

We similarly study output polarization multiplexing. Discrete dipole analysis, using the same library dimensions as in experiment, shows very similar trends as for input polarization multiplexing. Figure 2(f) shows ensemble error calculated versus photon budget for unpolarized input and readout, single-polarization input (H or V) and readout along the same polarization and for unpolarized input with H-V polarization resolved readout. Like for input polarization multiplexing, we see that single-polarization and unpolarized analysis perform similarly, but are outperformed by polarization-resolved readout. The effective improvement in photon budget is over 7 dB at a photon budget of 10^6. We test this prediction in experiment. Repeating our earlier experiments with output polarization multiplexing instead of input polarization multiplexing, we again see a significant improvement going from unpolarized measurements to H-V polarization resolved ones, as in Figs. 3(d) and 3(e). A series of such measurements across different devices (Fig. 3(f)) show the same trend as the theory: polarization-resolved analysis significantly outperforms the other strategies, confirming that, like input polarization multiplexing, output polarization multiplexing leads to more precise overlay retrieval.

Optics EXPRESS

At this point we ask how polarization channels relate to other possible information channels in causing the observed improvement in performance. We have so far considered quadrant detectors. Instead, we can analyze the calculated or measured radiation patterns at higher resolution in momentum space, keeping the detector pixel grid centered on the center of Fourier space and covering the same numerical aperture with more pixels. We calculate the theoretical photon budget, i.e. measurement time, required to obtain a certain maximum ensemble error. Several observations may be made about the results of these calculations for output polarization multiplexing, shown in Fig. 4(a). First, detectors with more pixels allow a given performance to be obtained at lower photon budget than those with fewer pixels. The largest advantage is seen going from just a few pixels to some tens, beyond which the improvements become smaller. This may be related to the number of effective degrees of freedom of the radiation patterns considered: the small size of our overlay targets means that their radiation patterns will be fairly smooth and may be reconstructed from fewer samples than would be needed to reconstruct the radiation patterns of extended structures. Another observation is that the polarization-resolved photon budget requirements are consistently lower than those for unpolarized measurement. This demonstrates that polarization multiplexing is advantageous over a wide range of photon budgets and detector resolutions (in pixels). One way to quantify this advantage is as effective noise reduction: the reduction in measurement time to obtain equal overlay retrieval performance when using (output) polarization multiplexed analysis instead of unpolarized analysis. We calculate effective noise reduction as a function of initial (unpolarized) photon budget, which is related to ensemble error as per the data in Fig. 2. This analysis is shown in Fig. 4(b). We see that effective noise reduction generally increases with photon budget. Few-pixel detectors are much more helped by polarization resolution than the high-resolution detectors that permit good overlay retrieval even without polarization resolution, as we saw from Fig. 4(a). Effective noise reduction at 10^6 photons appears to plateau at slightly more than 3 dB for anywhere between tens and thousands of pixels. With lower photon budgets, effective noise reduction decreases for all detector resolutions, but more strongly so for few-pixel detectors. These few-pixel detectors are much more error-prone with or without polarization resolution at these photon budgets, such that noise reduction at a photon budget of 10^5 is nearly independent of detector resolution. The 2 dB effective noise reduction in this regime still corresponds to an appreciable speed-up in measurement time for a given precision.

We can also use experimental data to analyze how greater detector resolution affects overlay retrieval performance. This is implemented experimentally by taking the original high-resolution camera images and dividing the region of interest into smaller superpixels than the quadrants considered before, thus incorporating more of the wavevector information into the camera images. In Fig. 4(c) we show the dependence of ensemble error on detector resolution for unpolarized measurement and output polarization multiplexed measurement. We see that performance improves rapidly with the number of pixels for small numbers of pixels but then plateaus, matching our expectation that the small scales involved would lead to broad features in Fourier images. Polarization resolution with a quadrant detector, for 8 degrees of freedom in total, provides performance between those of non-resolved detection with 9 and 16 degrees of freedom. We thus see that, one-for-one, the additional polarization-resolved degrees of freedom are more valuable in overlay retrieval than the additional wavevector degrees of freedom. We also see that a polarization-resolved 3×3 pixel detector outperforms non-resolved detection at many thousands of pixels. The precise numbers and degree of improvement are likely to depend on the details of the scattering problem under study. However, these data show that not all degrees of freedom are equally informative, polarization proving to be a particularly informative one on scattering systems such as those considered here.

Optics EXPRESS

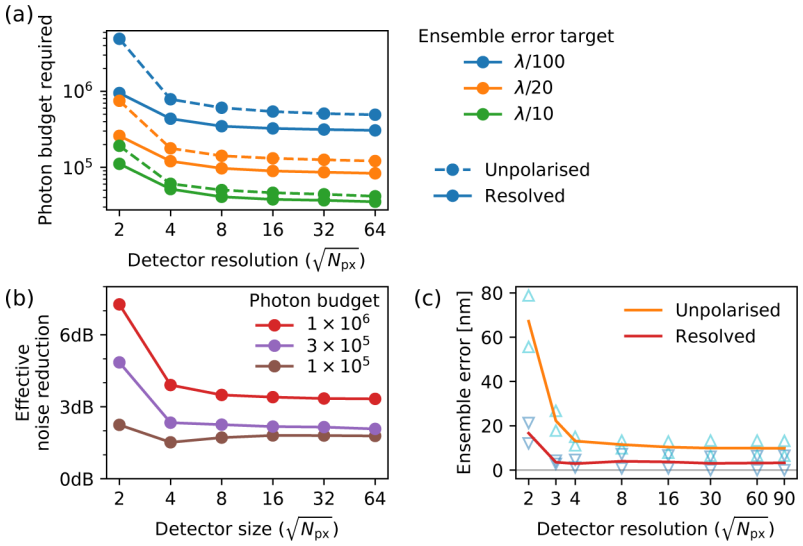

Fig. 4. Overlay retrieval performance versus detector resolution. (a) Theoretical required photon budget for given maximum ensemble error calculated for different detector resolutions. Solid lines indicate performance with polarization multiplexing, dashed lines without. (b) Theoretical effective noise reduction, the reduction in integration time to achieve a certain maximum ensemble error, calculated at different photon budget as a function of detector resolution. The detector resolution axis represents the number of pixels along one side of a square detector. (c) Experimental overlay retrieval performance versus detector resolution. Ensemble error as measured with different strategies, plotted versus detector resolution. Triangles show the experimental data averaged to obtain the lines.

4. Conclusion and discussion

We have explored how combining different polarization channels may assist nanophotonic parameter retrieval. Our results indicate that combining information from multiple polarization channels leads to significantly higher measurement precision than standard approaches in overlay retrieval on few-nanoparticle targets. Pairing different incident light polarizations and pairing different analysis polarizations both provide an improvement in effective photon budget of 7 dB or more, as compared with either unpolarized or single-polarization illumination and detection. These results are expected from discrete dipole theory, which predicts the advantage will persist over a wide range of photon budgets, and verified using experiments. Comparing polarization-multiplexed readout with additional degrees of freedom from higher wavevector resolution, we see that polarization resolution is particularly valuable, with a 3×3 detector with polarization multiplexing outperforming a non-polarization-resolved detector with many thousands of pixels.

It seems likely that polarization multiplexing can help in parameter retrieval not just for our few-particle overlay targets, but for any metrology problem where sample interactions are polarization-dependent, particularly in such applications as alignment and shape measurement. The technique may be particularly valuable for nanoscale scattering systems, which due to their size cannot encode information in fine features in scattering patterns. It would be interesting to explore which combinations of polarization channels would provide most information for a given target. Conversely, overlay targets may be designed for maximum sensitivity for given measurement conditions [43,44]. One may consider a similar multiplexing approach working based not on the polarization degree of freedom, but for instance on distinct incident wavevectors

Optics EXPRESS

or wavelengths, all of which may interact differently with samples. Further studies may investigate how these different degrees of freedom interact and complement one another in terms of sample information encoded. Multiplexing strategies like those tested here are particularly attractive because of their simplicity. Output polarization multiplexing in particular can be performed very easily and at minimal expense, requiring only a polarizing beam splitter and twice the camera pixels to introduce. As such, polarization multiplexing has the potential to enable more precise measurements in a myriad of applications.

Funding. Netherlands Organization for Scientific Research (NWO) (14669).

Acknowledgments. The authors thank Wim Coene for valuable discussions. This work is part of the research program of the Netherlands Organization for Scientific Research (NWO). It is part of the program High Tech Systems and Materials (HTSM) with Project No. 14669, which is (partly) financed by NWO.

Disclosures. The authors declare no conflicts of interest.

Data availability. Data underlying the results presented in this paper are not publicly available at this time but may be obtained from the authors upon reasonable request.

References

1. S. Alekseeva, I. I. Nedrygailov, and C. Langhammer, "Single particle plasmonics for materials science and single particle catalysis," ACS Photonics **6**(6), 1319–1330 (2019).
2. J. Xavier, D. Yu, C. Jones, E. Zossimova, and F. Vollmer, "Quantum nanophotonic and nanoplasmonic sensing: towards quantum optical bioscience laboratories on chip," Nanophotonics **10**(5), 1387–1435 (2021).
3. M. L. Tseng, Y. Jahani, A. Leitis, and H. Altug, "Dielectric metasurfaces enabling advanced optical biosensors," ACS Photonics **8**(1), 47–60 (2021).
4. J. Scheuer, "Optical metasurfaces are coming of age: Short- and long-term opportunities for commercial applications," ACS Photonics **7**(6), 1323–1354 (2020).
5. N. M. Felix, A. H. Gabor, V. C. Menon, P. P. Longo, S. D. Halle, C.-S. Koay, and M. E. Colburn, "Overlay improvement roadmap: strategies for scanner control and product disposition for 5-nm overlay," in *Metrology, Inspection, and Process Control for Microlithography XXV*, vol. 7971 C. J. Raymond, ed. (SPIE, 2011), pp. 432–438.
6. G. Yoo, J. Kim, C. Park, T. Lee, S. Ji, G. Jo, H. Yang, D. Yim, M. Yamamoto, K. Maruyama, and B. Park, "Real cell overlay measurement through design based metrology," in *Metrology, Inspection, and Process Control for Microlithography XXVIII*, vol. 9050 J. P. Cain and M. I. Sanchez, eds. (SPIE, 2014), pp. 468–478.
7. S. Kuiper, E. Fritz, W. Crowcombe, T. Liebig, G. Kramer, G. Witvoet, T. Duivenvoorde, T. Overtoom, R. Rijnbeek, E. van Zwet, A. van Dijsseldonk, A. den Boef, M. Beems, and L. Levasier, "Large dynamic range atomic force microscope for overlay improvements," in *Metrology, Inspection, and Process Control for Microlithography XXX*, vol. 9778 M. I. Sanchez and V. A. Ukraintsev, eds. (SPIE, 2016), pp. 438–447.
8. B. Bunday, E. Solecky, A. Vaid, A. F. Bello, and X. Dai, "Metrology capabilities and needs for 7nm and 5nm logic nodes," in *Metrology, Inspection, and Process Control for Microlithography XXXI*, vol. 10145 M. I. Sanchez and V. A. Ukraintsev, eds. (SPIE, 2017), pp. 102–142.
9. B. D. Bunday, A. Bello, E. Solecky, and A. Vaid, "7/5nm logic manufacturing capabilities and requirements of metrology," in *Metrology, Inspection, and Process Control for Microlithography XXXII*, vol. 10585 O. Adan and V. A. Ukraintsev, eds. (SPIE, 2018), pp. 81–124.
10. K. Bhattacharyya, "New approaches for scatterometry-based metrology for critical distance and overlay measurement and process control," J. Micro/Nanolithogr., MEMS, MOEMS **10**(1), 013013 (2011).
11. J. Benschop, A. Engelen, H. Cramer, M. Kubis, P. Hinnen, H. van der Laan, K. Bhattacharyya, and J. Mulkens, "Integrated scatterometry for tight overlay and CD control to enable 20-nm node wafer manufacturing," in *Optical Microlithography XXVI*, vol. 8683 W. Conley, ed. (SPIE, 2013), pp. 209–216.
12. N. Kumar, P. Petrik, G. K. P. Ramanandan, O. E. Gawhary, S. Roy, S. F. Pereira, W. M. J. Coene, and H. P. Urbach, "Reconstruction of sub-wavelength features and nano-positioning of gratings using coherent Fourier scatterometry," Opt. Express **22**(20), 24678–24688 (2014).
13. X. Chen, S. Liu, C. Zhang, and H. Jiang, "Measurement configuration optimization for grating reconstruction by Mueller matrix polarimetry," in *Metrology, Inspection, and Process Control for Microlithography XXVII*, vol. 8681 A. Starikov and J. P. Cain, eds. (SPIE, 2013), pp. 616–625.
14. J. M. Holden, T. Gubiotti, W. A. McGahan, M. V. Dusa, and T. Kiers, "Normal-incidence spectroscopic ellipsometry and polarized reflectometry for measurement and control of photoresist critical dimension," in *Metrology, Inspection, and Process Control for Microlithography XVI*, vol. 4689 D. J. C. Herr, ed. (SPIE, 2002), pp. 1110–1121.
15. M. H. Madsen and P.-E. Hansen, "Scatterometry—fast and robust measurements of nano-textured surfaces," Surf. Topogr.: Metrol. Prop. **4**(2), 023003 (2016).
16. J. H. Shapiro and R. W. Boyd, "The physics of ghost imaging," Quantum Inf. Process. **11**(4), 949–993 (2012).
17. J. N. Mait, G. W. Euliss, and R. A. Athale, "Computational imaging," Adv. Opt. Photonics **10**(2), 409–483 (2018).
18. J. Bertolotti, E. G. van Putten, C. Blum, A. Lagendijk, W. L. Vos, and A. P. Mosk, "Non-invasive imaging through opaque scattering layers," Nature **491**(7423), 232–234 (2012).

Optics EXPRESS

19. T. Wu, O. Katz, X. Shao, and S. Gigan, "Single-shot diffraction-limited imaging through scattering layers via bispectrum analysis," Opt. Lett. **41**(21), 5003–5006 (2016).
20. K. D. Unger, P. C. Chaumet, G. Maire, A. Sentenac, and K. Belkebir, "Versatile inversion tool for phaseless optical diffraction tomography," J. Opt. Soc. Am. A **36**(11), C1–C8 (2019).
21. T. Zhang, C. Godavarthi, P. C. Chaumet, G. Maire, H. Giovannini, A. Talneau, M. Allain, K. Belkebir, and A. Sentenac, "Far-field diffraction microscopy at λ/10 resolution," Optica **3**(6), 609–612 (2016).
22. D. Choudhury, D. K. McNicholl, A. Repetti, I. Gris-Sánchez, S. Li, D. B. Phillips, G. Whyte, T. A. Birks, Y. Wiaux, and R. R. Thomson, "Computational optical imaging with a photonic lantern," Nat. Commun. **11**(1), 5217 (2020).
23. J. L. Ponsetto, A. Bezryadina, F. Wei, K. Onishi, H. Shen, E. Huang, L. Ferrari, Q. Ma, Y. Zou, and Z. Liu, "Experimental demonstration of localized plasmonic structured illumination microscopy," ACS Nano **11**(6), 5344–5350 (2017).
24. R. Röhrich and A. F. Koenderink, "Double moiré localized plasmon structured illumination microscopy," Nanophotonics **10**(3), 1107–1121 (2021).
25. M. T. McCann, K. H. Jin, and M. Unser, "Convolutional neural networks for inverse problems in imaging: A review," IEEE Signal Process. Mag. **34**(6), 85–95 (2017).
26. A. Lucas, M. Iliadis, R. Molina, and A. K. Katsaggelos, "Using deep neural networks for inverse problems in imaging: Beyond analytical methods," IEEE Signal Process. Mag. **35**(1), 20–36 (2018).
27. Z. Lin, C. Roques-Carmes, R. Pestourie, M. Soljačić, A. Majumdar, and S. G. Johnson, "End-to-end nanophotonic inverse design for imaging and polarimetry," Nanophotonics **10**(3), 1177–1187 (2021).
28. D. Bouchet, J. Seifert, and A. P. Mosk, "Optimizing illumination for precise multi-parameter estimations in coherent diffractive imaging," Opt. Lett. **46**(2), 254–257 (2021).
29. F. Le Roy-Brehonnet and B. Le Jeune, "Utilization of Mueller matrix formalism to obtain optical targets depolarization and polarization properties," Prog. Quantum Electron. **21**(2), 109–151 (1997).
30. A. Aiello, G. Puentes, D. Voigt, and J. P. Woerdman, "Maximum-likelihood estimation of Mueller matrices," Opt. Lett. **31**(6), 817–819 (2006).
31. C. Fallet, "Overlay measurements by Mueller polarimetry in back focal plane," J. Micro/Nanolithogr., MEMS, MOEMS **10**(3), 033017 (2011).
32. A. Mohtashami, C. I. Osorio, and A. F. Koenderink, "Angle-resolved polarimetry of antenna-mediated fluorescence," Phys. Rev. Appl. **4**(5), 054014 (2015).
33. T. A. W. Wolterink, R. D. Buijs, G. Gerini, E. Verhagen, and A. F. Koenderink, "Calibration–based overlay sensing with minimal–footprint targets," Appl. Phys. Lett. **119**(11), 111104 (2021).
34. R. D. Buijs, N. J. Schilder, T. A. W. Wolterink, G. Gerini, E. Verhagen, and A. F. Koenderink, "Super-resolution without imaging: Library-based approaches using near-to-far-field transduction by a nanophotonic structure," ACS Photonics **7**(11), 3246–3256 (2020).
35. T. A. W. Wolterink, R. D. Buijs, G. Gerini, A. F. Koenderink, and E. Verhagen, "Localizing nanoscale objects using nanophotonic near-field transducers," Nanophotonics **10**(6), 1723–1732 (2021).
36. I. T. Jolliffe, *Principal Component Analysis* (Springer-Verlag, 2002).
37. L. Zhao, K. L. Kelly, and G. C. Schatz, "The extinction spectra of silver nanoparticle arrays: influence of array structure on plasmon resonance wavelength and width," J. Phys. Chem. B **107**(30), 7343–7350 (2003).
38. W. H. Weber and G. W. Ford, "Propagation of optical excitations by dipolar interactions in metal nanoparticle chains," Phys. Rev. B **70**(12), 125429 (2004).
39. M. Yurkin and A. Hoekstra, "The discrete dipole approximation: An overview and recent developments," J. Quant. Spectrosc. Radiat. Transfer **106**(1-3), 558–589 (2007).
40. P. C. Chaumet, T. Zhang, and A. Sentenac, "Fast far-field calculation in the discrete dipole approximation," J. Quant. Spectrosc. Radiat. Transfer **165**, 88–92 (2015).
41. L. Novotny and B. Hecht, *Principles of Nano-Optics* (Cambridge University Press, 2006).
42. F. J. García de Abajo, "Colloquium: Light scattering by particle and hole arrays," Rev. Mod. Phys. **79**(4), 1267–1290 (2007).
43. M. Adel, M. Ghinovker, B. Golovanevsky, P. Izikson, E. Kassel, D. Yaffe, A. Bruckstein, R. Goldenberg, Y. Rubner, and M. Rudzsky, "Optimized overlay metrology marks: theory and experiment," IEEE Trans. Semicond. Manuf. **17**(2), 166–179 (2004).
44. R. Röhrich, G. Oliveri, S. Kovaios, V. T. Tenner, A. J. den Boef, J. T. B. Overvelde, and A. F. Koenderink, "Uncertainty estimation and design optimization of 2d diffraction-based overlay metrology targets," ACS Photonics **7**(10), 2765–2777 (2020).